Scripta Materialia 177 (2020) 58–64

Contents lists available at ScienceDirect

Scripta Materialia

journal homepage: www.elsevier.com/locate/scriptamat

Nano-sized Cu clusters in deeply undercooled CoCuFeNiTa high entropy alloy

M.R. Rahul[a], Sumanta Samal[b], A. Marshal[c], V.I. Nithin Balaji[a], K.G. Pradeep[a], Gandham Phanikumar[a,*]

[a] Department of Metallurgical and Materials Engineering, Indian Institute of Technology Madras, Chennai 600036, India
[b] Discipline of Metallurgy Engineering and Materials Science, Indian Institute of Technology Indore, Simrol, Khandwa Road, Indore 453552, Madhya Pradesh, India
[c] Materials Chemistry, RWTH Aachen University, Aachen, Germany

ARTICLE INFO

Article history:
Received 18 August 2019
Revised 4 October 2019
Accepted 6 October 2019
Available online 18 October 2019

Keywords:
Undercooling
High entropy alloys
Growth velocity
Phase separation
Phase field simulation

ABSTRACT

The non-equilibrium response of a high entropy alloy $CoCuFeNiTa_{0.5}$ has been studied using undercooling as a control parameter. The solidification growth rates are rapid (30–50 m/s) at deep undercooling (>150 °C) and are comparable with conventional alloys. The elemental segregation especially that of Cu as predicted by phase field simulations in lower (<50 °C) undercooling regime matches with the experimental observations. This study indicates that even extreme non-equilibrium conditions during solidification could not avoid elemental segregation at the atomic scale.

The need for the development of new materials with improved structural and functional properties for application in energy, electronic and manufacturing sectors is often addressed by scientific studies through alloy design followed by microstructure-property optimisation. Research efforts in the past focused on developing alloys that can overcome fundamental challenges such as the strength-ductility trade off [1]. Recently, the design of a new class of alloys under the name “high entropy alloys” has led to the use of multiple principal elements which has widened the compositional space in search of new alloys exhibiting outstanding properties. Unlike conventional metallic alloys, the alloys with multiple principal elements/(HEAs)/complex concentrated alloys are at the central regions of the phase space. These alloys forming simple solid solution phases have shown exceptional properties including high strength as well as good ductility under different conditions [2–5].

Similar to conventional alloys, HEAs are also processed through non-equilibrium processing conditions such as additive manufacturing and melt spinning. The extent of non-equilibrium condition involved in the above processing methods is characterised by undercooling viz., the difference between the liquidus temperature of the alloy and the nucleation temperature achieved during the process. Undercooling dependent morphological changes and segregation of elements are established in binary alloys such as Fe–Ni [6] and Cu–Ni systems [7]. Reports on such explorations in HEAs is, however, limited [8,9]. Rapid cooling rates obtained for example during physical vapour deposition techniques such as magnetron sputtering of the CoCrCuFeNi HEA helped avoid segregation of elements and a single phase solid solution was obtained [10]. Detailed transmission electron microscopy of splat quenched AlCoCrCuFeNi HEA confirmed metastable bcc phase formation suppressing the otherwise expected equilibrium phases [11]. However, undercooling studies on CoCrCuFeNi HEA showed phase separation during solidification challenging the concept of high entropy stabilized solid solution formation phenomena [8,9,12]. On the other hand, it is also difficult to generalise that the diffusion of elements in HEAs is sluggish where predominant phase separation has been reported after prolonged annealing treatments [13,14]. To this extent, the most pertinent question that remains unanswered is whether extreme non-equilibrium conditions can aid in suppressing segregation in high entropy alloys.

To address the above question, the alloy $CoCuFeNiTa_{0.5}$ was subjected to deep undercooling (up to 0.20 T_L (Liquidus temperature) ≈250 °C) using melt flux technique that included a high-speed camera for solidification growth rate measurement and in-situ non-contact measurement of the temperature of the sample.

* Corresponding author.
E-mail address: gphani@iitm.ac.in (G. Phanikumar).

https://doi.org/10.1016/j.scriptamat.2019.10.006
1359-6462/

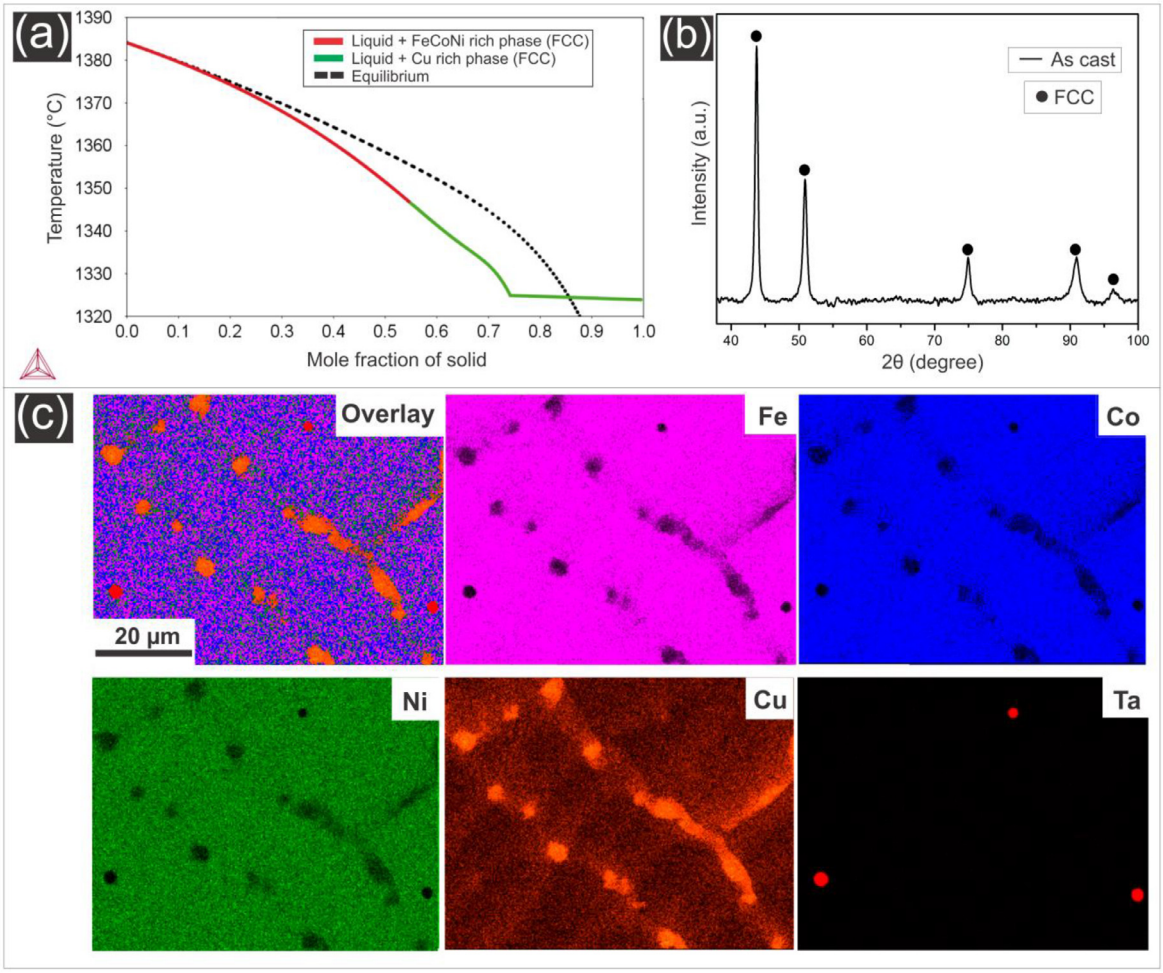

Fig. 1. (a) Thermo-Calc® prediction of $CoCuFeNiTa_{0.5}$ alloy using TCHEA1 database where the red line shows the FCC FeCoNi rich phase and green line shows the Cu rich FCC phase predicted by scheil's equation and the dotted line indicates the equilibrium prediction, (b) XRD pattern of as cast sample, (c) EDS mapping of as-cast $CoCuFeNiTa_{0.5}$ alloy (Ta is 0.5 atomic percentage and other elements in equiatomic composition). (For interpretation of the references to colour in this figure legend, the reader is referred to the web version of this article.)

Segregation behaviour of elements was predicted at smaller undercooling using phase field simulation. Finally, we explore if deep undercooling can suppress the segregation tendency of Cu overcoming positive enthalpy of mixing with the rest of the elements in the selected HEA.

The alloy $CoCuFeNiTa_{0.5}$ was melted in the form of 30 g button using vacuum arc melting technique. Undercooling studies were carried out in a sealed chamber filled with high purity argon gas and by placing the sample in a quartz tube with boron trioxide flux. Thermal profile during solidification was measured using a non-contact two colour infrared pyrometer. In situ measurement of recalescence velocity was performed using high-speed video imaging using Photron FASTCAM® high-speed camera. The metallographically prepared samples were characterised using a scanning electron microscope (SEM) (InspectF® and FEI Helios Nanolab 660) in backscattered electron mode while the compositional analysis was performed using EDS (EDAX®). XRD measurements were performed in X'pert Pro PANalytical® setup for phase identification. To study the elemental distribution at near-atomic resolution, APT (using LEAP 4000X HR from Cameca Inc®) measurement was carried out on deeply undercooled sample ($\Delta T = 235$ °C). APT measurements were performed in a laser-pulsed mode with an applied pulse energy of 30 pJ at 250 kHz frequency while the tip was maintained at 60 K. Data reconstruction and analysis was performed using IVAS 3.8.2 software provided by CamecaInc®. Samples for APT and Transmission electron microscopy (TEM) (Tecnai-FEI®) imaging were prepared using a dual-beam workstation, FEI Helios Nanolab 660.

Phase-field simulation of microstructure evolution was carried out using MICRESS® software. Liquid phase and primary dendrite (FCC) phases were considered for simulation with a grid spacing of 0.3 µm. Solute partitioning at the interface as a function of temperature and composition was available by TQ® coupling with the thermodynamic data available in the TCHEA1 database in Thermo-Calc®. The governing equation used was the following phase field model implemented in MICRESS® software.

$$\frac{\partial \Phi}{\partial t} = \mu^*(\vec{n})\left[\sigma^*(\vec{n})\left(\nabla^2\Phi + \frac{\pi^2}{\eta^2}\left(\Phi - \frac{1}{2}\right)\right) + \frac{\pi}{\eta}\sqrt{\Phi(1-\Phi)}\Delta G\right]$$

here, Φ is the phase field order parameter, $\mu^*(\vec{n})$ is the anisotropic interfacial mobility, η is the diffuse interface thickness, $\sigma^*(\vec{n})$ is the anisotropic interfacial energy, and ΔG is the Gibbs energy as driving force. Further details of the model are published elsewhere [15–17].

In $CoCuFeNiTa_{0.5}$ alloy, the elements Fe, Co and Ni have a negative enthalpy of mixing and hence the propensity to form a solid solution [18,19]. Segregation effects arising from a positive enthalpy of mixing with Cu are investigated to decipher the role of

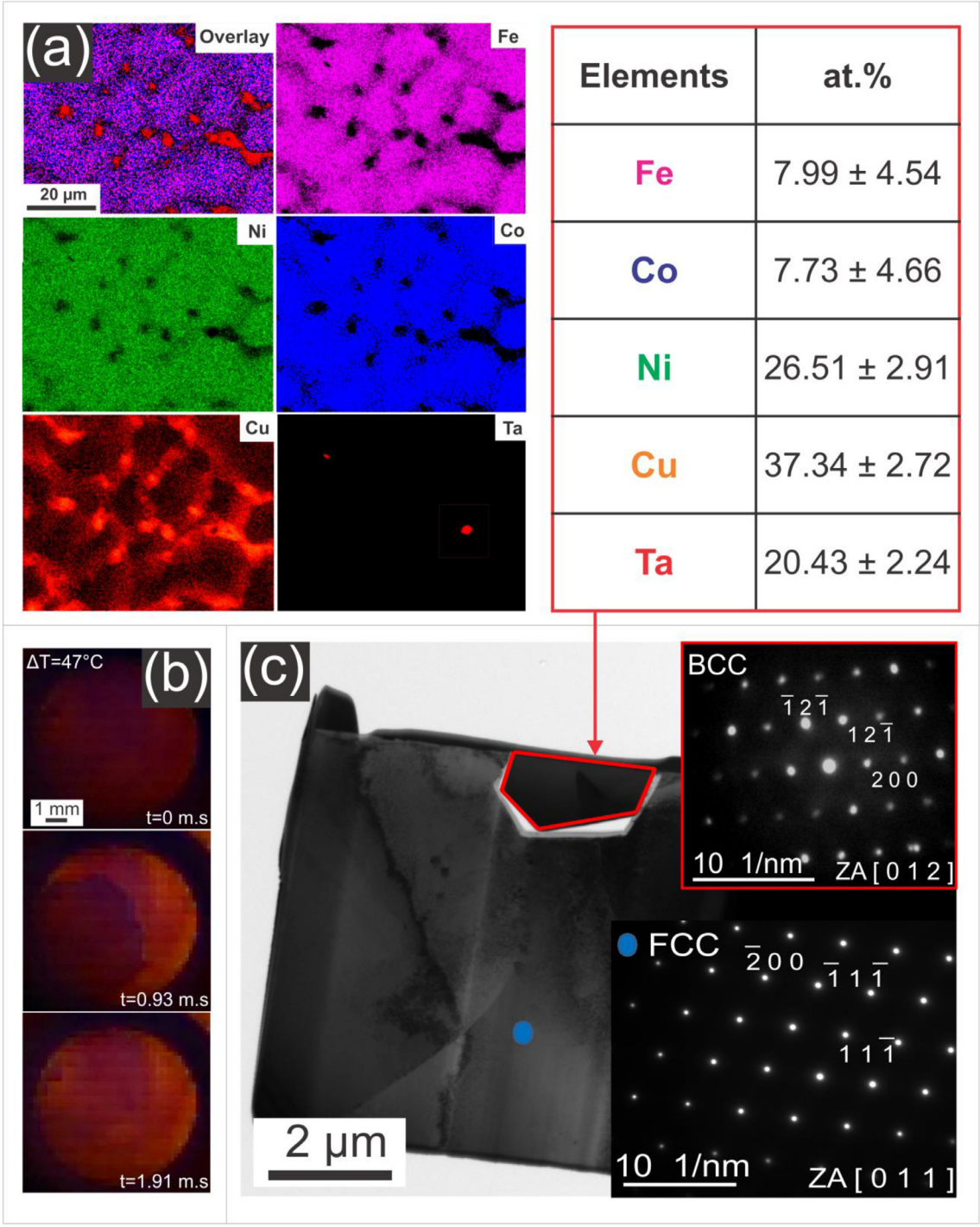

Fig. 2. (a) EDS mapping of undercooled sample at $\Delta T = 47$ °C and the table shows the composition of Ta rich phase, (b) Snapshots of high speed video imaging of undercooled sample at $\Delta T = 47$ °C, (c) TEM image of undercooled sample at $\Delta T = 47$ °C undercooling shows Ta rich phase with BCC crystal structure.

extreme non-equilibrium conditions achieved by deep undercooling. A heavy element, Ta was intentionally added in small quantity to suppress the kinetics during undercooling. Scheil's solidification pathway from thermodynamic estimates shows the formation of two phases (Fig. 1a) viz., FeCoNi rich phase and Cu rich phase during solidification.

XRD pattern of the as-cast sample in Fig. 1b confirms the major phase to be of FCC crystal structure. The SEM-EDS map (Fig. 1c) indicates chemical inhomogeneity with preferential segregation of Ta and Cu at selective regions such as grain boundaries. Table 1 shows the average composition obtained by the EDS measurement at different regions. The major phase formed is FCC structured FeCoNi rich as per the thermodynamic prediction. The EDS mapping also shows the segregation of Cu in the interdendritic region with a length scale of 4–5 μm.

Deep undercooling could lead to the formation of metastable phases along with suppression of elemental partitioning as evident from studies on traditional alloys [20–23]. The initial observation on the presence of multiple phases in the as-cast state of the investigated alloy requires further understanding of the role of

Table 1
EDS composition of different phases found at as-cast $FeCoNiCuTa_{0.5}$ sample.

Regions	Fe	Co	Ni	Cu	Ta
FeCoNi rich phase	27.22 ± 2.49	24.58 ± 2.29	29.24 ± 2.66	18.13 ± 3.49	0.83 ± 26.35
Cu rich region	10.77 ± 4.02	9.95 ± 4.07	14.93 ± 3.00	61.89 ± 2.12	2.46 ± 15.99
Ta rich region	14.32 ± 6.43	11.82 ± 6.69	12.19 ± 6.31	8.85 ± 8.01	52.82 ± 2.67

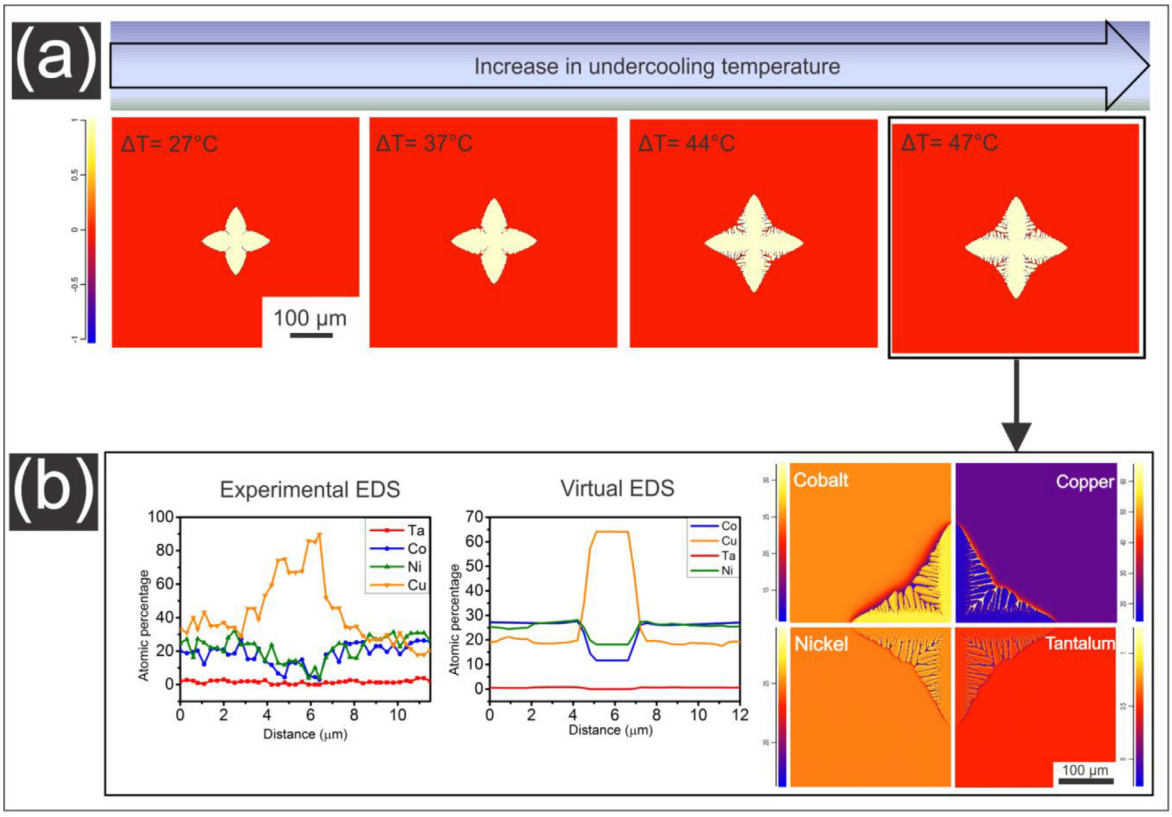

Fig. 3. (a) Phase field simulation plots of undercooled sample microstructure at different undercooling level (time step = 0.1 s), (b) Segregation profile and line scan comparison of constituent elements at ΔT = 47 °C undercooling (time step = 0.15 s).

kinetics in phase formation during undercooling. Microstructure evolution of $CoCuFeNiTa_{0.5}$ can be understood in two regimes namely small undercooling (<150 °C) and deep undercooling (>150 °C).

Fig. 2a shows the EDS mapping of the sample obtained at an undercooling temperature of 47 °C and it exhibits three distinct regions of segregation namely, Ta rich, Cu rich and the FeCoNi rich matrix. The quantitative composition analysis of the Ta-rich phase by EDS indicates the presence of a solid solution type configuration consisting of Ta, Ni and Cu which is different from the as-cast condition (supplementary figure S2). The selected snapshots of high-speed camera images shown in Fig. 2b enable visualisation of solidification process during recalescence using thermal contrast. The image shown in Fig. 2b has an angular front, which is characteristic of the low undercooling domain. TEM image obtained in bright field mode performed on a sample prepared site-specifically from a Ta-rich region shows that the Ta-rich phase has BCC crystal structure (Fig. 2c). The matrix phase is FCC solid solution enriched with FeCoNi. Ta has a large negative enthalpy of mixing (−29 kJ/mol) with Ni and explains the resulting enrichment of Ni in this phase [19]. The results indicate that the small undercooling employed is not sufficient enough to suppress the formation of multiple phases.

The segregation behaviour of the alloy under study was predicted using phase field modelling at different undercooling temperatures. Fig. 3a shows phase field plot at the same time step keeping all parameters constant. The increasing trend in velocity was comparable to the experimental studies. At 27 °C undercooled condition, the phase field plot shows primary dendritic arms while increasing the undercooling to 47 °C leads to the formation of secondary arms. Segregation behaviour of the small (47 °C) undercooled sample, is shown in Fig. 3b. Cu is segregated in the interdendritic region, while Co and Ni are concentrated on the primary dendrites. Ta appears to be slightly more enriched in the dendritic region while the difference with respect to interdendritic region is not appreciable compared to the case of Cu or Ni or Co. The quantitative interdendritic segregation profile obtained in the form of elemental distribution along a line for both experimental and simulated (virtual EDS) conditions is shown in Fig. 3b. The line profiles are in good agreement with each other highlighting the applicability of phase field predictions for real microstructure evolution. At large undercoolings (ΔT = 235 °C) the phase field simulations using simulation package have shown instability as the Gibbs energy functions needed a better description for their extrapolation. It is to be noted that the Cu segregation was reported in CoCrFeNiCu alloy during directional solidification where the primary dendritic arm spacing and secondary dendritic arm spacing decreases with increase in solidification velocity [24]. The segregation length scale in directional solidification was less than ~5 μm and the current study the as cast and lower undercooling region the Cu segregated

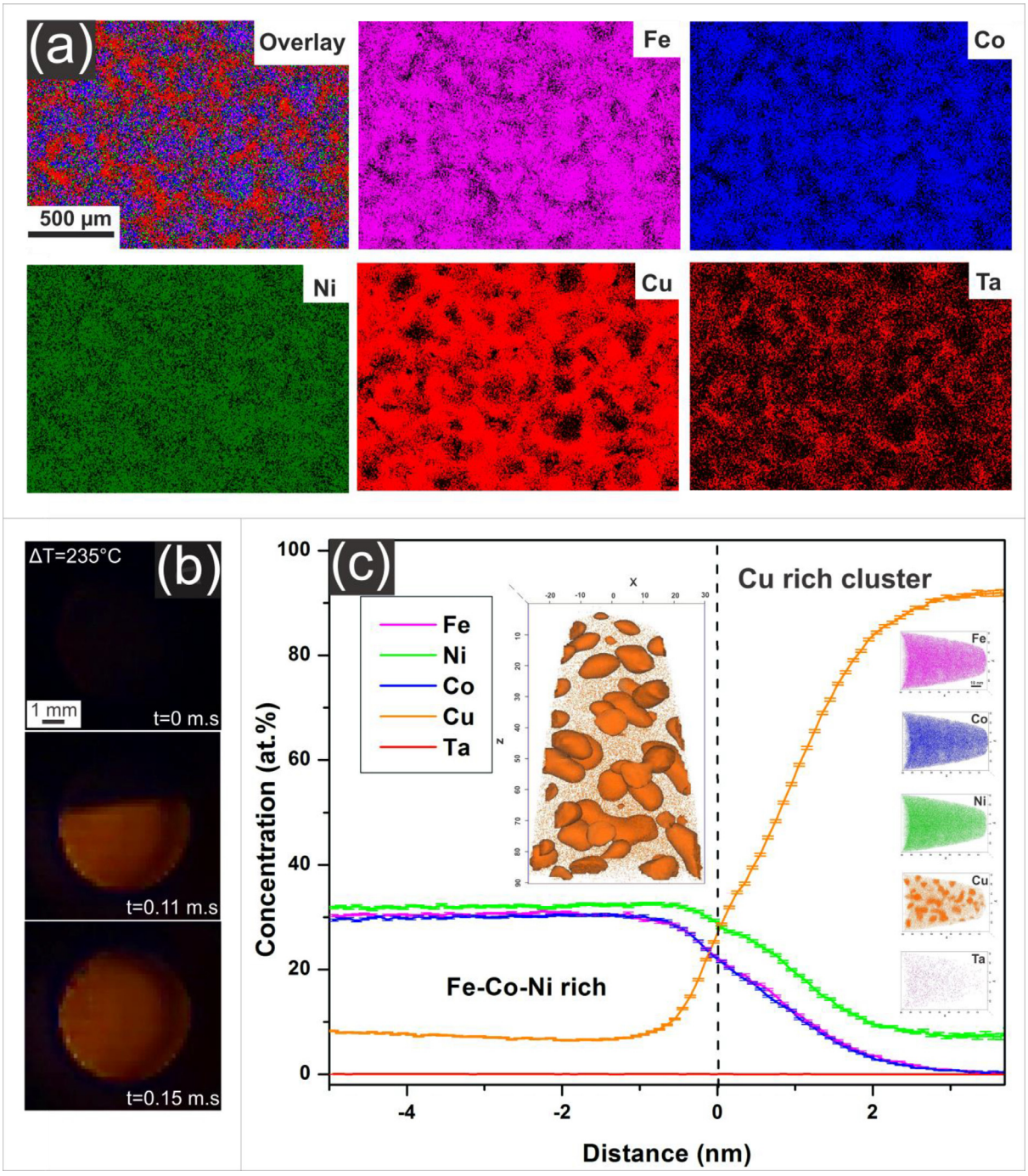

Fig. 4. (a) SEM EDS mapping of undercooled sample at ΔT = 235 °C, (b) Snapshots of high speed video imaging of sample at ΔT= 235 °C shows smooth solid liquid interface, (c) atomic distribution and concentration profile of 235 °C undercooled sample. (d) Dendritic growth velocity of undercooled sample obtained from high speed video analysis (Fig. S3) shown as experimental data, blue line shows the data fit by power law equation where growth velocity (v) = 0.0234 $(\Delta T)^{1.3567}$, red line show the dendritic growth velocity predicted by dendritic growth model. (For interpretation of the references to colour in this figure legend, the reader is referred to the web version of this article.)

with a scale of ~ 4 μm which decreases with increase in undercooling.

From the EDS maps (Fig. 4a), it is evident that Ta enriched region was suppressed during deep undercooling. The spherical front imaged by the high-speed camera (Fig. 4b) is due to the deep undercooling achieved. The three-dimensional elemental distribution at the near-atomic scale using APT of a deeply undercooled (ΔT = 235 °C) sample is shown in Fig. 4c.

The elemental distribution map of Cu with clusters (segregation) delineated from the matrix using 25 at.% Cu isoconcentration surface within the $60 \times 61 \times 91$ nm^3 volume is shown in the inset of Fig. 4c. Cu clusters of about 10–15 nm in size were found in the analysed volume after solidification. The formation of nano scale precipitates was reported in CoCrCuMnNi non equiatomic system where they observed the Co–Cr rich precipitates with a diameter range of 3–8 nm [25]. Ta appears to be distributed randomly in the analysed volume. Fe, Ni and Co are depleted in the Cu rich region as which is further confirmed using the statistical proximity histogram (Fig. 4c) obtained from all of the delineated Cu rich clusters. The FeCoNi rich region in the proxigram corresponds to

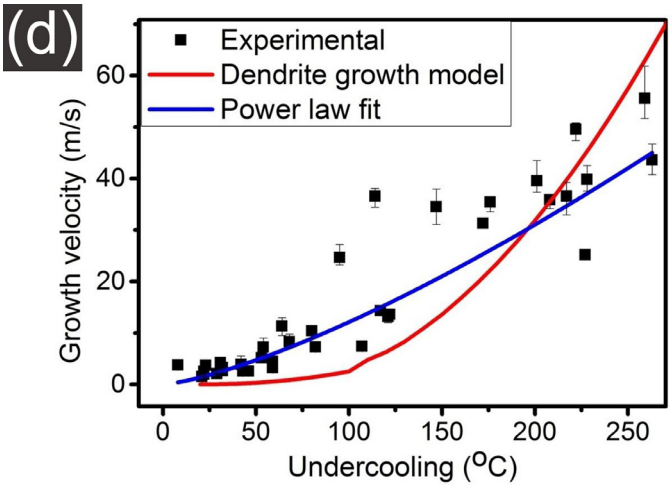

Fig. 4. Continued

the matrix FCC phase as was also predicted by thermodynamic calculations.

Measurement of recalescence speed during solidification of undercooled melts using a high-speed camera often provides insights into the magnitude of the kinetics of phase formation. The recalescence front was tracked using a high-speed camera with 10^5 frames per second to measure the velocity data (supplementary Fig. S3). The variation of dendrite growth speed as a function of the extent of undercooling (Fig. 4d) shows an increasing trend as expected in conventional alloys [26] such as Ni-based alloys [23,27,28] and other multi-component alloys [17]. The growth data shows a steep change marking a transition from small undercooling to deep undercooling. This is often attributed to the transition from the dominance of solute contribution to the overall undercooling to kinetic contribution [29]. The variation of growth velocity can be fitted either to a nonlinear function of the undercooling temperature or a dendrite growth model using pseudo-binary approach considering that copper is the main segregating element. Using the parameters listed in table S1 (supplementary file), it can be concluded that the growth rates are similar to conventional alloys and not sluggish.

Deep undercooling effect on the microstructure evolution of $CoCuFeNiTa_{0.5}$ connects the various length scales of segregation behaviour, i.e., the extent of phase separation of constituent elements. Cu has a positive enthalpy of mixing and is immiscible with Fe and Co resulting in Cu rich FCC phase in the as-cast alloy. 3D APT result confirms that the apparently phase pure interdendritic regions when observed at SEM resolution are actually phase separated at near atomic-scale. The formation of Cu clusters in highest undercooled condition may due to the formation of supersaturated solid solution. Here, the primary phase contained mainly of Fe, Co and Ni. It is possible that during solidification at deep undercooling, solute trapping leads to the primary phase containing more Cu content than equilibrium. During the subsequent cooling, some of the Cu precipitates out and is in nano meter scale and are not easily identified in routine electron microscopy.

The elemental distribution across length scales from microns to a nanometer regime exemplifies the extent of segregation even in deep undercooling condition. This implies that in $CoCuFeNiTa_{0.5}$ HEA extreme undercooling condition was not sufficient to suppress the phase separation. This is an unexpected observation given that in HEAs, formation of solid solution phases are expected particularly when solute trapping could aid the same at deeper undercooling. The experimentally observed growth velocity (30–50 m/s) at higher undercooling indicates that the alloy can exhibit phase-pure microstructure due to solute trapping, which was not observed on the contrary. Solute trapping is a prominent effect in traditional alloys (with a single principal element) in undercooled conditions [17,29]. The literature shows that in the Fe based quaternary alloys, the solute will have noticeable effect below critical undercooling levels [30]. The effect of minute additions of Al and Zr in Ni on growth velocity shows growth rates of 25 m/s to 40 m/s at deep undercooling (>175 °C) [17]. Multi solute trapping is possible in multicomponent alloys in the undercooled conditions, but the $CoCuFeNiTa_{0.5}$ alloy shows a growth rate variation comparable to traditional dilute alloys. The growth velocity variation as a function of undercooling can be modelled using dendritic growth models. The dendrite growth models take into account different undercooling contributions. The kinetic undercooling can be defined as $\Delta T_k = \mu(v/v_c)$ where μ = kinetic coefficient, v = Dendrite tip velocity, v_c = maximum possible growth rate which is taken as the velocity of sound. For complex systems, the velocity of solid-liquid interface is often related to undercooling using power law equation. In this study, we could fit the experimental data to the dendrite growth model using non-linear kinetics $\Delta T_k = \mu(v/v_c)^{0.55}$. While it is possible to further refine the growth models for accuracy, but based on the current results, it can be concluded that growth rates are rapid at deep undercooling and have significant kinetic effects in this alloy system.

The present study on undercooled $CoCuFeNiTa_{0.5}$ HEA demonstrates that the hypothesis of stabilisation of solid solution phase when configurational entropy is sufficiently large may not be universally valid– particularly when melt route is used for alloy preparation. While deep undercooling could promote suppression of certain additional phases, the resultant effect would then be ascribed to solute trapping effects typical of non-equilibrium solidification. Observation of phase separation at the near-atomic scale suggests that kinetics could lower the extent of phase separation but cannot avoid it altogether.

Declaration of Competing Interest

The authors declare that they have no known competing financial interests or personal relationships that could have appeared to influence the work reported in this paper.

Acknowledgements

Rahul M R acknowledges Nithin B, PhD scholar in Department of Metallurgical and Materials Engineering, IIT Madras for helping in TEM studies.

Supplementary material

Supplementary material associated with this article can be found, in the online version, at doi:10.1016/j.scriptamat.2019.10.006.

References

[1] Z. Li, K.G. Pradeep, Y. Deng, D. Raabe, C.C. Tasan, Nature 534 (2016) 227–230.
[2] O.N. Senkov, J.D. Miller, D.B. Miracle, C. Woodward, Nat. Commun. 6 (2015) 6529:1–10.
[3] Y. Zou, H. Ma, R. Spolenak, Nat. Commun. 6 (2015) 7748:1–8.
[4] Y.H. Jo, S. Jung, W.M. Choi, S.S. Sohn, H.S. Kim, B.J. Lee, N.J. Kim, S. Lee, Nat. Commun. 8 (2017) 15719: 1–8.
[5] R.S. Ganji, P. Sai Karthik, K. Bhanu Sankara Rao, K.V. Rajulapati, Acta Mater. 125 (2017) 58–68.
[6] J.F. Li, W.Q. Jie, G.C. Yang, Y.H. Zhou, Acta Mater 50 (2002) 1797–1807.
[7] T. Zhang, F. Liu, H.F. Wang, G.C. Yang, Scr. Mater. 63 (2010) 43–46.
[8] N. Liu, P.H. Wu, P.J. Zhou, Z. Peng, X.J. Wang, Y.P. Lu, Intermetallics 72 (2016) 44–52.
[9] T. Guo, J. Li, J. Wang, Y. Wang, H. Kou, S. Niu, Intermetallics 86 (2017) 110–115.
[10] Z. An, H. Jia, Y. Wu, P.D. Rack, A.D. Patchen, Y. Liu, Y. Ren, N. Li, P.K. Liaw, Mater. Res. Lett. 3 (2015) 203–209.
[11] S. Singh, N. Wanderka, B.S. Murty, U. Glatzel, J. Banhart, Acta Mater. 59 (2011) 182–190.
[12] A. Munitz, M.J. Kaufman, R. Abbaschian, Intermetallics 86 (2017) 59–72.
[13] M. Vaidya, S. Trubel, B.S. Murty, G. Wilde, S.V. Divinski, J. Alloys Compd. 688 (2016) 994–1001.
[14] F. Otto, A. Dlouhý, K.G. Pradeep, M. Kubenova, D. Raabe, G. Eggeler, E.P. George, Acta Mater 112 (2016) 40–52.
[15] B. Böttger, J. Eiken, M. Apel, Comput. Mater. Sci. 108 (2015) 283–292.
[16] J. Eiken, B. Böttger, I. Steinbach, Phys. Rev. E - Stat. Nonlinear, Soft Matter Phys. 73 (2006) 1–9.
[17] P.K. Galenko, S. Reutzel, D.M. Herlach, S.G. Fries, I. Steinbach, M. Apel, Acta Mater. 57 (2009) 6166–6175.
[18] A.R. Miedema, F.R. de Boer, R. Boom, Calphad 1 (1977) 341–359.
[19] A. Takeuchi, A. Inoue, Mater. Trans. 46 (2005) 2817–2829.
[20] J. Gao, T. Volkmann, J. Strohmenger, D.M. Herlach, Mater. Sci. Eng. A 375-377 (2004) 498–501.
[21] D.M. Herlach, J. Gao, D. Holland-Moritz, T. Volkmann, Mater. Sci. Eng. A 375-377 (2004) 9–15.
[22] J. Gao, T. Volkmann, D.M. Herlach, Acta Mater. 50 (2002) 3003–3012.
[23] K. Eckler, F. Gärtner, H. Assadi, A.F. Norman, A.L. Greer, D.M. Herlach, Mater. Sci. Eng. A 226-228 (1997) 410–414.
[24] H. Zheng, R. Chen, G. Qin, X. Li, Y. Su, H. Ding, J. Guo, H. Fu, J. Mater. Sci. Technol. (2019) in press.
[25] G. Qin, R. Chen, P.K. Liaw, Y. Gao, X. Li, H. Zheng, L. Wang, Y. Su, J. Guo, H. Fu, Scr. Mater. 172 (2019) 51–55.
[26] J. Valloton, D.M. Herlach, H. Henein, D. Sediako, Metall. Mater. Trans. A Phys. Metall. Mater. Sci. 48 (2017) 4735–4743.
[27] K. Eckler, D.M. Herlach, Mater. Sci. Eng. 178 (1994) 159–162.
[28] D.M. Herlach, S. Binder, P. Galenko, J. Gegner, D. Holland-Moritz, S. Klein, M. Kolbe, T. Volkmann, Metall. Mater. Trans. A Phys. Metall. Mater. Sci. 46 (2015) 4921–4936.
[29] G. Phanikumar, K. Biswas, O. Funke, D. Holland-Moritz, D.M. Herlach, K. Chattopadhyay, Acta Mater 53 (2005) 3591–3600.
[30] Y. Ruan, F.P. Dai, Intermetallics 25 (2012) 80–85 30 pJ.